Paper 3

AN ANALYSIS OF THE DYNAMICS OF AUTOMOBILES DURING SIMULTANEOUS CORNERING AND RIDE MOTIONS

By R. R. McHenry*

A mathematical model of an automobile is described, which permits the study of simultaneous cornering and ride motions on irregular terrain. A major departure from previous analytical treatments of vehicles is abandonment of the concept of a vehicle-fixed 'hinge' to approximate the changing virtual axis about which roll takes place.

Eleven degrees of freedom and all major non-linearities are included in the equations of motion, which are programmed for time-history solutions on a digital computer. Empirical relationships used to generate tyre forces over extreme ranges of operating conditions are presented in detail. To ease the task of interpretation of the extensive output information, a computer-graphics display technique has been developed to produce detailed perspective drawings of the vehicle and terrain at selected intervals of time during a simulated manoeuvre.

Comparisons are presented of analytically predicted vehicle responses and test results. Future applications of the described mathematical model, in research related to highway safety, are briefly discussed.

INTRODUCTION

THE VEHICLE MOTIONS of interest in the present study are those that occur immediately prior to and during accidental departures from the roadway. Such motions generally include large deviations from a reference condition of steady rectilinear motion. Since the large deviations frequently occur simultaneously in the longitudinal and lateral modes of motion, it has been necessary to include general three-dimensional motions in the developed mathematical model of vehicle dynamics. It has also been necessary to include the major non-linearities of the vehicle and to provide for easily adjustable terrain and obstacle properties.

The development of an appropriate analytical representation of an automobile has required a departure from earlier practice in the co-ordinate axis system for the vehicle (1)† (2) (3). In the present study, the position and orientation of the vehicle-fixed co-ordinate axes (Fig. 3.1) correspond to a direct application of the conventional practice of aircraft stability and control analysis (4) to the sprung mass portion of the automobile. The selected analytical representation of the automobile abandons the concept of a vehicle-fixed 'hinge' to approximate the changing virtual axis about which roll actually takes place. Constraints are imposed on motions of the unsprung masses, relative to the sprung mass of the simulated vehicle, such that a realistic and changing virtual axis is generated for roll motions.

It should be noted that the cited earlier analyses of automobile dynamics have had objectives which were substantially different from those of the present research and which have both permitted and made desirable the incorporation of extensive simplifications. For example, linearized three-degree-of-freedom equations have been shown to be both accurate and useful for analysis of small-disturbance handling qualities of automobiles on flat, horizontal terrain (1) (2). Also, a recent study of the dynamics of the automobile in relation to response characteristics of the driver–vehicle closed-loop system (3) cites the advantages of linearized equations from the viewpoint of the applicability of operational calculus and servo-analysis methods.

The mathematical model that is described herein requires the use of a large-capacity computer (e.g. an IBM 360-65) to obtain solutions for the equations of

The MS. of this paper was received at the Institution on 18th October 1968 and accepted for publication on 30th October 1968.

* *Head, Engineering Mechanics Section, Transportation Research Department, Cornell Aeronautical Laboratory, Inc., Buffalo, New York, U.S.A.*

† *References are given in Appendix 3.3.*

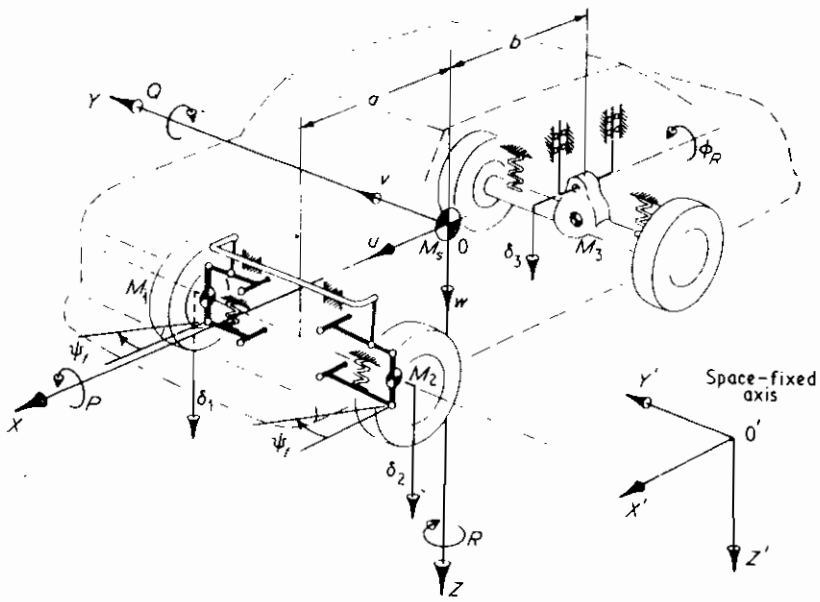

Fig. 3.1. Analytical representation of vehicle

motion. Once such a dependence on computer solutions is accepted, the need for and the desirability of analytical simplifications become primarily matters of economics. An acceptable compromise must be achieved between the accuracy of analytical representation and the costs of development and operation of the computer programme. The downwards trend in computer operating costs in recent years (Fig. 3.2, (5)) has shifted the required compromise towards greater analytical detail.

The selection of analytical simplifications in the present study has been somewhat biased by an emphasis on the prediction of collision responses. The treatment of details related to handling characteristics has, therefore, been aimed at adequacy rather than a high degree of accuracy. Examples of pertinent simplifications are the adoption of the 'friction circle' concept, the assumption of equal front wheel steer angles, and the neglect of roll–steer effects in the front suspension. Despite these recognized analytical inaccuracies, a high degree of correlation has been achieved between predicted and experimental responses in a variety of vehicle manoeuvres. The relatively inexpensive operating costs of the computer programme in its present form (approximately \$5.00 per second of simulated time, in non-impact runs) make the development of a non-impact version of the programme, with improved details for handling studies, a particularly attractive prospect.

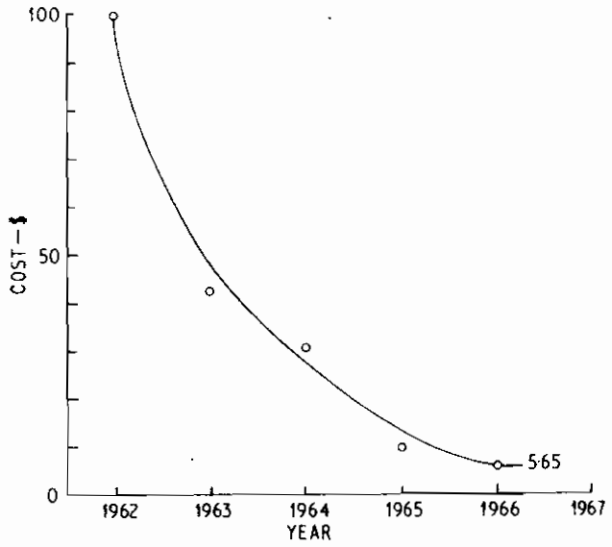

Operating cost of a computer programme that cost \$100 per run in 1962.

For 'large scientific computers' (5).

Fig. 3.2. Computer costs versus years

This paper describes the mathematical model, giving emphasis to the non-impact aspects, and presents comparisons of predicted and experimental responses. Empirical relationships used to generate tyre forces are presented in detail. A computer-graphics display technique, which has been developed to ease the task of interpretation of the extensive output information, is also described. Comparisons are then presented of predicted and experimental vehicle responses. Included in the comparisons are computer-graphics perspective drawings of the simulated vehicle for viewing positions and times corresponding to those of individual frames taken from high-speed films of experiments. Appendix 3.1 presents a summary of equations related to side, braking, and traction forces of the tyres. Appendix 3.2 contains a listing of the vehicle parameter values that have been used in the presented response predictions.

Notation

$A_0, \ldots, A_4$ Constant coefficients in parabolas fitted to tyre side force properties.

a, b Distances along the vehicle-fixed X-axis from the sprung mass centre of gravity to the centre-lines of the front and rear wheels, respectively, in (see Fig. 3.1).

C_{C_0} Small-angle camber stiffness, lb/rad.

C_{S_0} Small-angle cornering stiffness, lb/rad.

F_{C_i} Circumferential tyre force (i.e. traction or braking) at wheel i, lb.

F'_{C_i} Value of circumferential tyre force that is used in approximating the effects of differential gears, at wheel i, lb (see Appendix 3.1).

F_{R_i} Radial tyre force at wheel i, lb.

F'_{R_i} Tyre force perpendicular to the tyre–terrain contact plane at wheel i, lb.

F_{S_i} Tyre side force in the plane of the tyre–terrain contact patch, perpendicular to the line of intersection of the wheel and ground planes at wheel i, lb.

F'_{S_i} Tyre side force for small slip angles and for 'equivalent' slip angles that approximate camber effects, at wheel i, lb.

$(F_{S_i})_{\max}$ Maximum possible tyre side force at wheel i, lb.

h_i Rolling radius of wheel i, in.

I_X, I_Y, I_Z, I_{XZ} Moments and products of inertia of sprung mass, lb s^2 in.

I_R Rear unsprung mass moment of inertia about a line through its centre of gravity and parallel to the X-axis, lb s^2 in.

i 1, 2, 3, 4, corresponding to RF, LF, RR, and LR wheels, respectively.

K_T Radial tyre rate in quasi-linear range for a single tyre, lb/in (see Fig. 3.4).

$M_1 = M_2$ Front unsprung mass at a single wheel, lb s^2/in.

M_3 Rear unsprung mass, lb s^2/in.

M_S Sprung mass, lb s^2/in.

P, Q, R Scalar components of sprung mass angular velocity, taken along the X, Y, Z axes, respectively, rad/s.

R_W Undeflected radius of wheels, in.

T_i Circumferential tyre force corresponding to the applied torque at wheel i, which is subjected to force-limiting logic, lb.

$\overline{TQ}_F, \overline{TQ}_R$ Tabular inputs of applied torque for a single wheel, effective at the wheel, for front and rear wheels, respectively (positive for traction, negative for braking), lb ft.

u, v, w Scalar components of linear velocity of the sprung mass, taken along the X, Y, Z axes, respectively, in/s.

u_{G_i} Forward velocity of wheel centre i in the direction parallel to the tyre–terrain contact plane, in/s.

$|u_{G_i}|$ Absolute value of u_{G_i}.

$1 \text{ sgn } u_{G_i}$ Algebraic sign of u_{G_i}.

v_{G_i} Lateral velocity of the contact point of wheel i in the direction parallel to the tyre–terrain contact plane, in/s.

Z'_{G_i} Ground elevation with respect to the space-fixed Z'-axis, under the centre of wheel i, in.

Z'_{G_i} A vector through the ground contact point, normal to the actual or 'equivalent' tyre–terrain contact plane, at wheel i (see Fig. 3.5).

β_i Slip angle at wheel i, rad.

β'_i 'Equivalent slip angle' produced by camber effects at wheel i, rad.

$\bar{\beta}_i$ Non-dimensional slip angle variable for wheel i.

$f(\bar{\beta}_i)$ Non-dimensional side force at wheel i.

$\delta_1, \delta_2, \delta_3$ Suspension deflections relative to the vehicle from the positions of static equilibrium, at the right front wheel centre, left front wheel centre, and rear axle roll centre, respectively, in.

ζ_3, ζ_4 Suspension deflections relative to the vehicle from the positions of static equilibrium, at the right rear wheel centre and left rear wheel centre, respectively, in.

θ_{G_i}, ϕ_{G_i} Euler angular co-ordinates of terrain profile relative to the space-fixed co-ordinate system, under the centre of wheel i, rad.

λ_T Multiple of K_T for use in non-linear range of tyre deflection (i.e. travel limit, see Fig. 3.4).

μ, μ_C Friction coefficients for tyre–ground and tyre–kerb contacts, respectively.

σ_T Maximum radial tyre deflection for quasi-linear load deflection characteristics (see Fig. 3.4).

ϕ_R Angular displacement of the rear axle relative to the vehicle about a line parallel to the X-axis through the rear axle roll centre (positive when clockwise as viewed from the rear), rad.

ϕ_{CG_i} Camber angle of wheel i relative to its tyre–terrain contact plane, rad.

ψ'_i Steer angle of wheel i in its tyre–terrain contact plane, rad.

ψ_F Steer angle of front wheels relative to vehicle axis system, positive for clockwise steer as viewed from above vehicle (assumed equal at the two wheels), rad.

Ω_T Multiple of A_2 at which the assumed parabolic variations of small-angle cornering and camber stiffnesses are abandoned to preclude reversal in the sign of the side force (see Fig. 3.7).

DESCRIPTION OF MATHEMATICAL MODEL

Degrees of freedom

The vehicle is treated as an assembly of four rigid masses, as depicted in Fig. 3.1, with a total of 10 degrees of freedom in which inertial interactions are simulated. A steer mode degree of freedom, ψ_F, for which any inertial coupling effects are neglected, is introduced at the front wheels when rigid obstacles (e.g. kerbs) are encountered by the wheels.

The steer angle at the front wheels, ψ_F, is treated as an arbitrary tabular function of time prior to wheel contact with a rigid obstacle. The tabular values at the time of contact and immediately prior to that time are used to provide starting values of angular displacement and velocity for the steer degree of freedom.

The centres of gravity of the front unsprung masses are assumed to be constrained to move along straight-line paths that are parallel to the sprung mass Z-axis. The centre of gravity of the rear unsprung mass is assumed to be constrained to motions in a plane that is perpendicular to the sprung mass X-axis, and it is additionally assumed to be constrained to remain a fixed distance from the rear axle 'roll centre' (i.e. the virtual centre about which axle motions take place in roll). The rear axle roll centre is assumed to be constrained to move along a straight-line path parallel to the sprung mass Z-axis.

It is recognized that the actual paths, on the vehicle, of the unsprung mass centres of gravity are curvilinear; however, the errors in inertial interaction effects produced by the straight-line assumptions are considered to be negligible. The corresponding errors in suspension geometry, for which corrections could readily be incorporated, are also considered to be negligible for the present purposes of the simulation.

Inertial properties

Plane OXZ in Fig. 3.1 is assumed to be a plane of mirror symmetry for the sprung mass.

The centres of gravity of the front unsprung masses are assumed to coincide with the wheel centres. The front wheels are treated as point masses.

The centre of gravity of the rear unsprung mass is assumed to coincide with the geometric centre of the rear axle. In the treatment of inertial coupling between the sprung mass and the rear unsprung mass, the rear axle is approximated by a thin rod.

Gyroscopic effects of the rotating wheels, drive train, and engine are neglected.

Suspension geometry

Camber angles of the individual front wheels relative to the vehicle are determined by interpolation of a tabular input of camber angle as a function of suspension deflection (i.e. δ_1 and δ_2 in Fig. 3.1).

The steer angles of the front wheels relative to the vehicle are assumed to be equal. Roll steer effects in the front suspension are neglected.

Rear axle roll steer is treated as a linear function of the angular degree of freedom of the rear axle, ϕ_R (see Fig. 3.1). Inertial effects are neglected in the steer mode of rear axle motion.

Anti-pitch effects are approximated by means of coefficients that are entered separately for the front and rear suspensions as tabular functions of the suspension deflections. The product of the wheel torque (braking or traction) at a given wheel and the appropriate anti-pitch coefficient for that wheel and its suspension deflection is applied as a positive or negative 'jacking' effect on the suspension at the given wheel.

External forces

The simulation includes external forces that are applied either to the tyre–terrain contact patches or, in collisions with obstacles, directly to the sprung mass. Aerodynamic forces and rolling resistance are neglected.

TYRE PROPERTIES

It is entirely feasible in a digital computer programme of this type to enter measured tyre data in tabular form and to interpolate the tabular entries to obtain forces and moments corresponding to the instantaneous operating conditions. However, in view of the secondary emphasis placed on detailed tyre properties in the present version of the simulation, fitted empirical relationships have been developed to simplify the input requirements and to conserve core storage capacity for use in routines related to sprung mass impact.

The developed simulation of the tyres is designed to handle the complete range of tyre loading, from a loss of ground contact to conditions of extreme overload. The empirical relationships used to generate the side, braking, and traction forces are aimed primarily at accuracy within the normal ranges of operating conditions. It is assumed that excursions beyond the normal ranges of operating conditions will be of limited duration and that the tyre forces under those conditions can be treated in a more approximate manner. The selection of this method of approach was also prompted by the dearth of applicable data for tyres under the extremes of operating conditions.

One important point should be made before discussion of the assumptions regarding tyre properties under extreme operating conditions. In a computer programme of this type, provision must be made for all conceivable combinations of conditions. The logic and equations of the calculation programme must include comprehensive instructions, regardless of the existence of gaps in presently available information.

Radial loading

As a starting point in the tyre force calculations, the radial loading of each tyre, F_{Ri}, is first calculated from the position and orientation of the individual wheel in relation to the local terrain. The radial loading is calculated in

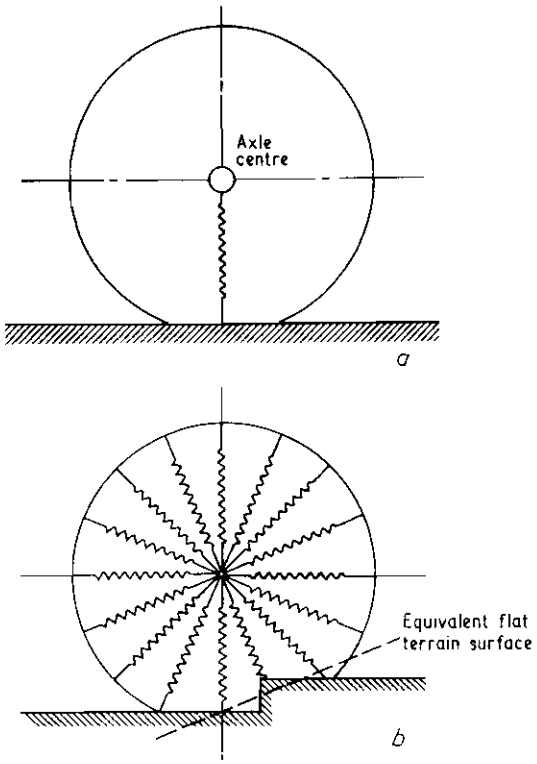

a Point contact model of tyre.
b Distributed contact radial spring model of tyre.

Fig. 3.3. Two modes of simulation of the radial characteristics of tyres

two different modes, depending on the nature of the tyre–terrain contact patch (see Fig. 3.3).

In the first mode, terrain undulations are assumed to be sufficiently gradual to produce essentially planar tyre–terrain contact patches at the individual tyres. Within this mode, a 'point-contact' representation of the tyre is used to generate the radial loading. At each point in time, the terrain elevations and slopes, at points directly under each wheel centre, are obtained by interpolation of tabular input data for the terrain profile (see 'Terrain profile' below). Determination of the 'ground contact points' is accomplished by passing planes through the wheel centre perpendicular to both the wheel and the local ground planes at the individual wheels. At each wheel, the point that lies in all three planes is designated the 'ground contact point'. The distances between the individual wheel centres and the corresponding 'ground contact points' are then calculated to determine the existence and the extent of radial tyre deflections. A 'hardening' spring characteristic, depicted in Fig. 3.4, is applied to generate corresponding radial loadings for the individual tyres.

The second mode of radial load calculation is used in the case of terrain irregularities for which the tyre–terrain contact patch is not planar (e.g. kerbs). In this mode, the individual wheels that are in contact with such a terrain irregularity are treated as discs with non-linear radial

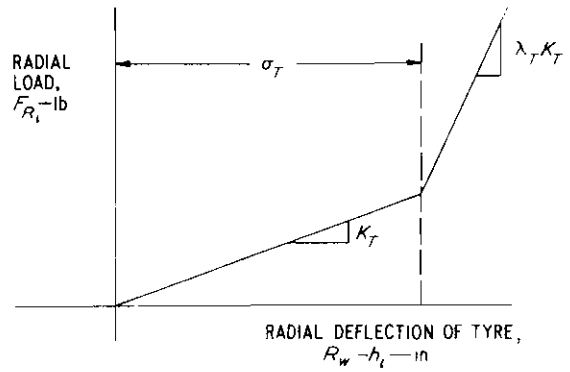

Fig. 3.4. Assumed radial load deflection characteristics of tyres, flat terrain

springs, as proposed in reference (**6**). The non-linear radial springs are arbitrarily spaced 4 degrees apart in the assumed wheel disc, and they are given identical load-deflection characteristics, which are automatically generated by an input subroutine to match the specified (input data) flat-terrain properties of the point-contact mode (Fig. 3.4). At each point in time, the lower half of the wheel plane is swept by a vector, with origin at the wheel centre and length equal to the undeflected wheel radius, to determine the tyre–terrain interface profile at the locations of the individual radial springs. The vector sum of radial forces, corresponding to the deflections and orientations of the individual springs, is used to generate an 'equivalent' ground contact point and an 'equivalent' flat terrain surface at each wheel, thereby permitting a continuous calculation of approximate side, traction, and braking forces. The 'equivalent' flat terrain surfaces are established by the use, as a normal to the 'equivalent' flat surface, of the projection of the normal to the actual terrain at the 'equivalent' ground contact point into the plane determined by the resultant radial force vector and a normal to the wheel plane (see Fig. 3.5). In this manner, the line of intersection between the 'equivalent' ground plane and the wheel plane is made to remain perpendicular to the resultant radial tyre force vector, while compatibility with the actual terrain slope is maintained.

Side, braking, and traction forces

Tyre loading normal to the ground contact patch

The side, braking, and traction forces are, of course, related to the tyre load normal to the plane of the tyre–terrain contact patch, F'_{R_i}, rather than to the radial tyre load, F_{R_i}. Therefore, it is necessary to find the value of F'_{R_i} corresponding to the radial load, F_{R_i}, and the side force, F_{S_i}. In Fig. 3.6, the components of the external applied forces, F'_{R_i} and F_{S_i}, along the line of action of the radial tyre force, F_{R_i}, are depicted. These force components must be in equilibrium with F_{R_i}, such that

$$F'_{R_i} \cos \phi_{CG_i} + F_{S_i} \sin \phi_{CG_i} = F_{R_i} \quad . \quad (3.1)$$

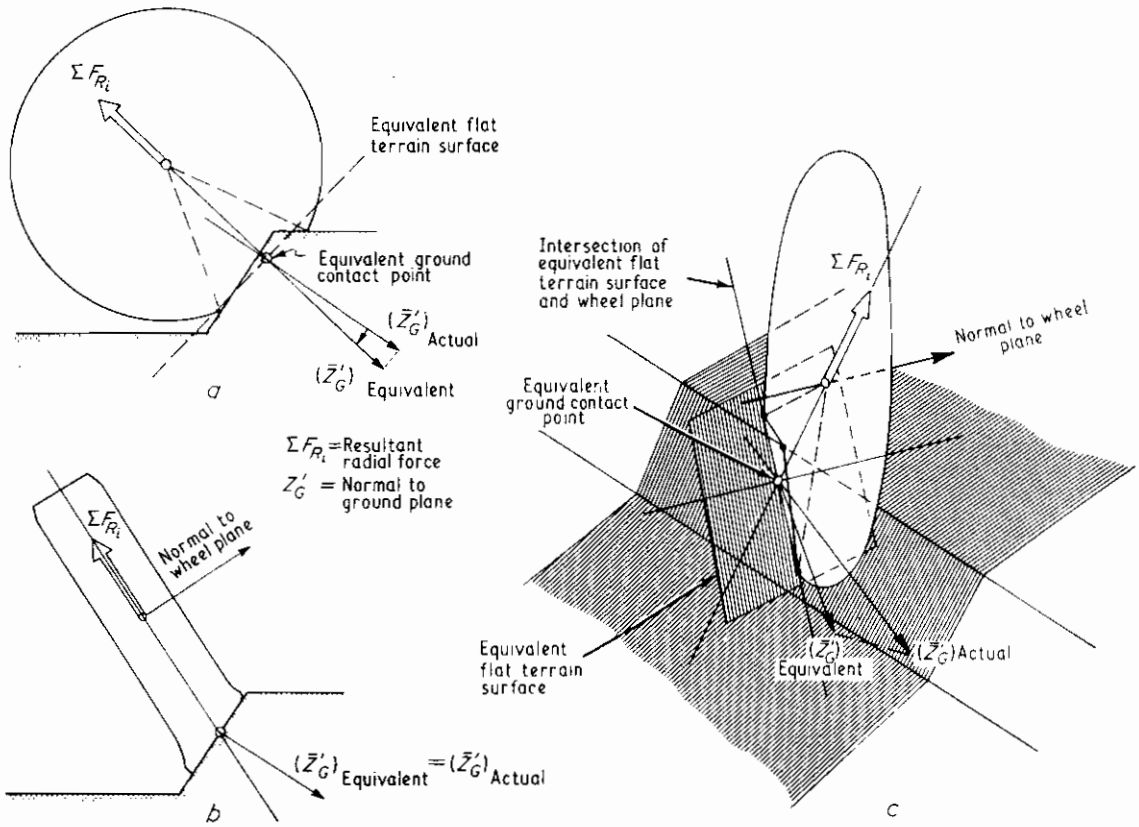

a Case 1. Wheel plane perpendicular to obstacle profile.
b Case 2. Wheel plane parallel to obstacle profile.
c Case 3. Oblique contact with terrain irregularity.

Fig. 3.5. 'Equivalent' flat terrain surface for non-planar tyre–terrain contact

The solution of equation (3.1) for F'_{R_i} yields

$$F'_{R_i} = F_{R_i} \sec \phi_{CG_i} - F_{S_i} \tan \phi_{CG_i} \quad . \quad (3.2)$$

Since F'_{R_i} is required for the determination of F_{S_i}, an initial approximation of F_{S_i} is obtained by extrapolation from the previous time increment. Following the calculation of F_{S_i} in the current time increment, an iterative procedure is employed to correct both F'_{R_i} and F_{S_i}.

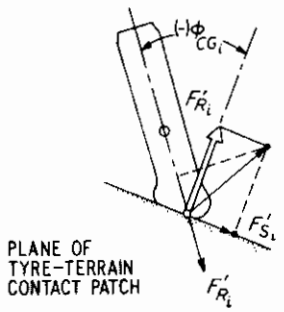

ϕ_{CG_i} Camber angle relative to terrain (shown negative).
F_{S_i} Side force produced by combination of slip angle and camber angle.
i 1, 2, 3, 4.

Fig. 3.6. Vector summation of forces with components along the line of action of the radial tyre force (viewed from rear)

Effects of loading on side forces

The side force calculations are based on the small-angle properties of the tyres which are 'saturated' at large angles. Variations in the small-angle cornering and camber stiffnesses, which are produced by changes in tyre loading, are approximated by parabolic curves fitted to experimental data (Fig. 3.7). The small-angle cornering stiffness is taken to be the partial derivative of lateral force with respect to slip angle as measured at zero slip angle for various tyre loads. The upper plot in Fig. 3.7 depicts a parabola fitted to the small-angle cornering stiffness as a function of tyre loading, in which the cornering stiffness is

$$C_{S_0} = A_0 + A_1 F'_{R_i} - \frac{A_1}{A_2} (F'_{R_i})^2 \quad . \quad (3.3)$$

The lower plot of Fig. 3.7 depicts a similar fit to small-angle camber stiffness, the partial derivative of lateral force with respect to camber angle as measured at zero camber angle, in which the camber stiffness is

$$C_{C_0} = A_3 F'_{R_i} - \frac{A_3}{A_4} (F'_{R_i})^2 \quad . \quad . \quad (3.4)$$

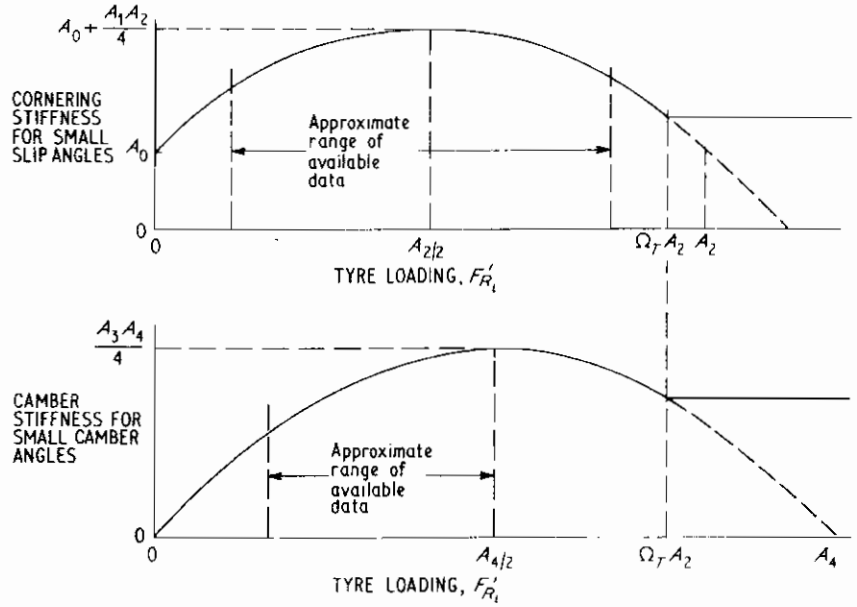

A_0, A_1, A_2, A_3, A_4 = Constants in fitted parabolas.

Fig. 3.7. Simulated variation of small-angle cornering and camber stiffness with loading normal to tyre–terrain contact patch

It should be noted that the constant term in equation (3.3) was found to be required to achieve a satisfactory fit to the relatively extensive experimental data provided by the General Motors [illegible] for the cornering stiffness of the 8·25-14 tyres that have been used in experiments within this research programme. A similar constant term may eventually be found to be desirable in equation (3.4). However, the available camber stiffness data are less extensive, and they do not warrant a corresponding programme modification at the present time.

The fitted parabolic curves are abandoned for tyre loading in excess of $\Omega_T A_2$ (see Fig. 3.7), where the approximate range of the coefficient is $0{\cdot}80 < \Omega_T < 1{\cdot}15$ (Ω_T is an adjustable item of input data), and the side force properties are then treated as being independent of tyre loading. The use of Ω_T was found to be necessary to avoid artificial reversal of the slip angle forces under conditions of extreme loading (i.e. where $A_2 \ll F'_{R_i}$). Actual properties of tyres in this range of loading (i.e. extreme overload) are not known.

Calculation of side forces

The general analytical approach of reference (7), wherein application is made of a non-dimensional slip angle variable and the 'friction circle' concept, has been adapted to suit the needs of the present simulation. Modifications were necessary to approximate the effects of camber and load changes and to provide for the occurrence of large slip angles and reversals in vehicle velocity. The resulting analytical treatment of the tyre forces is outlined in the following paragraphs.

For the case of zero traction and braking, the side forces, for small slip and camber angles, can be expressed, from equations (3.3) and (3.4), as

$$(F_{S_i})_{\text{camber}} = -\left[\frac{A_3F'_{R_i}(F'_{R_i}-A_4)}{A_4}\right]\phi_{CG_i} \quad . \quad . \quad (3.5)$$

$$(F_{S_i})_{\text{slip}} = \left[\frac{A_1F'_{R_i}(F'_{R_i}-A_2)-A_0A_2}{A_2}\right]\left[\frac{v_{G_i}}{u_{G_i}}-\psi'_i\right] \quad . \quad . \quad . \quad (3.6)$$

where the sign convention corresponds to the right-hand rule applied to the system depicted in Fig. 3.1.

The present simulation must handle extremely large camber angles relative to the tyre–terrain contact planes (e.g. see bridge parapet impact in the 'Discussion of results' which includes camber angles in excess of 80°). Since applicable tyre data are not known to be available, the assumption has been made that the camber force, for a given normal load, will reach its maximum value at 45° of camber. In accordance with this assumption, a parabolic variation of camber force with camber angle is simulated, with the peak occurring at 45° (see Fig. 3.8). With the assumed large-angle camber characteristic (depicted in

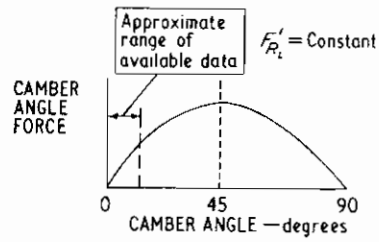

Fig. 3.8. Assumed variation of camber force with camber angle

Fig. 3.8), equation (3.5), for the complete range of possible camber angles, becomes

$$(F_{Si})_{\text{camber}} = -\left[\frac{A_3 F'_{Ri}(F'_{Ri}-A_4)}{A_4}\right]\left[\phi_{CGi}-\frac{2}{\pi}\phi_{CGi}\,|\phi_{CGi}|\right] \quad . \quad . \quad . \quad (3.7)$$

To permit the use of the non-dimensional slip angle concept of reference (7), which 'saturates' the side force at large slip angles, an 'equivalent' slip angle is defined to approximate camber effects:

$$\beta'_i = \left\{\frac{A_2A_3F'_{Ri}(A_4-F'_{Ri})}{A_4[A_1F'_{Ri}(F'_{Ri}-A_2)-A_0A_2]}\right\} \times\left[\phi_{CGi}-\frac{2}{\pi}\phi_{CGi}\,|\phi_{CGi}|\right] \quad (3.8)$$

Note that the selected analytical treatment of camber angles subjects the camber force to the 'saturation' effects of the slip angle, superimposed on the assumed behaviour shown in Fig. 3.8. While the assumption depicted in Fig. 3.8 is probably in error, it was found to be necessary to reduce the 'equivalent' slip angle of large camber angles to avoid an unrealistic predominance of camber effects on steeply inclined terrain obstacles. On the basis of the comparisons of predicted and experimental responses that have been made to date, it must be concluded that the selected analytical representation of large-angle camber effects is at least adequate.

Using definition (3.8), the resultant side force, for small slip angles and the entire range of camber angles, can be expressed as

$$F'_{Si} = \left[\frac{A_1F'_{Ri}(F'_{Ri}-A_2)-A_0A_2}{A_2}\right]\left[\frac{v_{Gi}}{u_{Gi}}-\psi'_i+\beta'_i\right] \quad . \quad . \quad . \quad (3.9)$$

Application of equation (3.9) to the non-dimensional side force relationship of reference (7) (see Fig. 3.9) yields

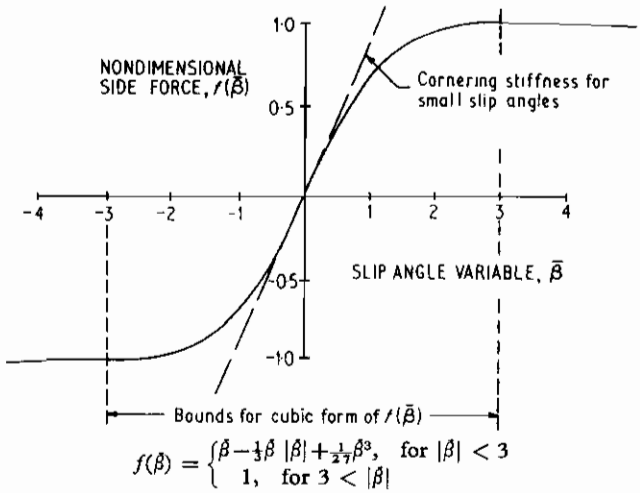

Fig. 3.9. Non-dimensional tyre side force curve

$$f(\bar{\beta}_i) = \frac{F_{Si}}{(F_{Si})_{\max}} = \bar{\beta}_i-\tfrac{1}{3}\bar{\beta}_i\,|\bar{\beta}_i|+\tfrac{1}{27}\bar{\beta}_i^3 \quad (3.10)$$

where F_{Si} is the resultant side force, for entire range of slip and camber angles, and

$$\bar{\beta}_i = \frac{F'_{Si}}{(F_{Si})_{\max}} \quad . \quad . \quad . \quad (3.11)$$

Large values of the slip angle, particularly in skidding, make it necessary to use the arctan (v_{Gi}/u_{Gi}) rather than v_{Gi}/u_{Gi}. Also, in cases where reversal of the vehicle velocity has occurred, it has been found to be necessary to control the algebraic signs of the slip and steer angles, so that equation (3.11) requires a modified form of equation (3.9), as follows:

$$\bar{\beta}_i = \left[\frac{A_1F'_{Ri}(F'_{Ri}-A_2)-A_0A_2}{A_2(F_{Si})_{\max}}\right] \times\left[\arctan\frac{v_{Gi}}{|u_{Gi}|}-(1\ \text{sgn}\ u_{Gi})\psi'_i+\beta'_i\right] \quad (3.12)$$

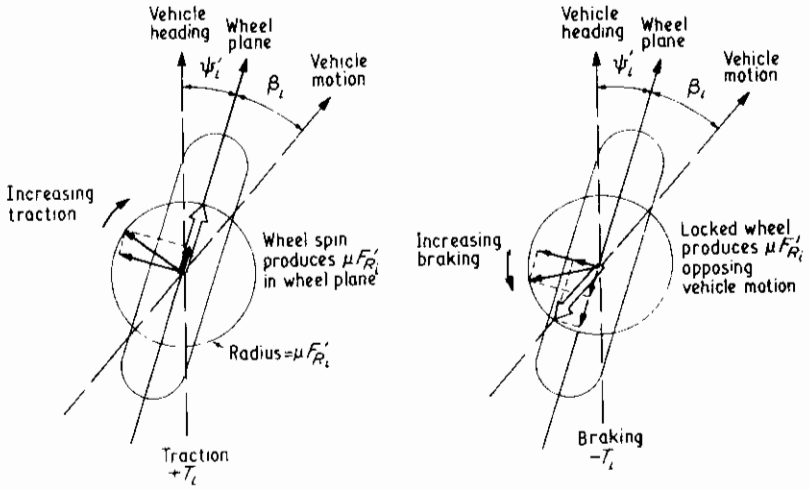

$\beta_i = \left[\arctan\frac{v_G}{|u_{Gi}|}-(1\ \text{sgn}\ u_{Gi})\psi'_i\right]$ = slip angle in tyre-terrain contact plane.

Fig. 3.10. Friction circle concept

Effects of traction and braking

The 'friction circle' concept is based on the assumption that the maximum force that can be generated by the tyres in the plane of the tyre–terrain contact patch is equal in all directions. While there is experimental evidence to indicate that this assumption is not accurate [e.g. reference (8)], it was considered to be adequate for the present purposes. It should be noted that the nature of the present computer programme permits relatively easy adjustment of the force-generating subroutines, so that a future version of the programme, aimed specifically at handling characteristics, could readily incorporate improved accuracy in the generation of tyre forces. With the use of the 'friction circle' concept (see Fig. 3.10), the maximum side force can be expressed as

$$(F_{Si})_{\max} = \sqrt{[\mu^2(F'_{Ri})^2 - F_{Ci}{}^2]} \quad . \quad (3.13)$$

where F_{Ci} is the circumferential tyre force (i.e. traction or braking) at wheel i, in pounds.

A summary of equations related to side, braking, and traction forces is presented in Appendix 3.1. In view of the relatively complex treatment of those tyre forces, plots of the resulting characteristics are presented in Figs 3.11 and 3.12.

Wheel aligning torques

Aligning torques on the front wheels are simulated by means of a constant 'pneumatic trail' dimension when the steer-mode degree of freedom is activated.

Tyre pressures

Properties of the front and rear tyres are assumed to be identical functions of tyre loading. There has been no

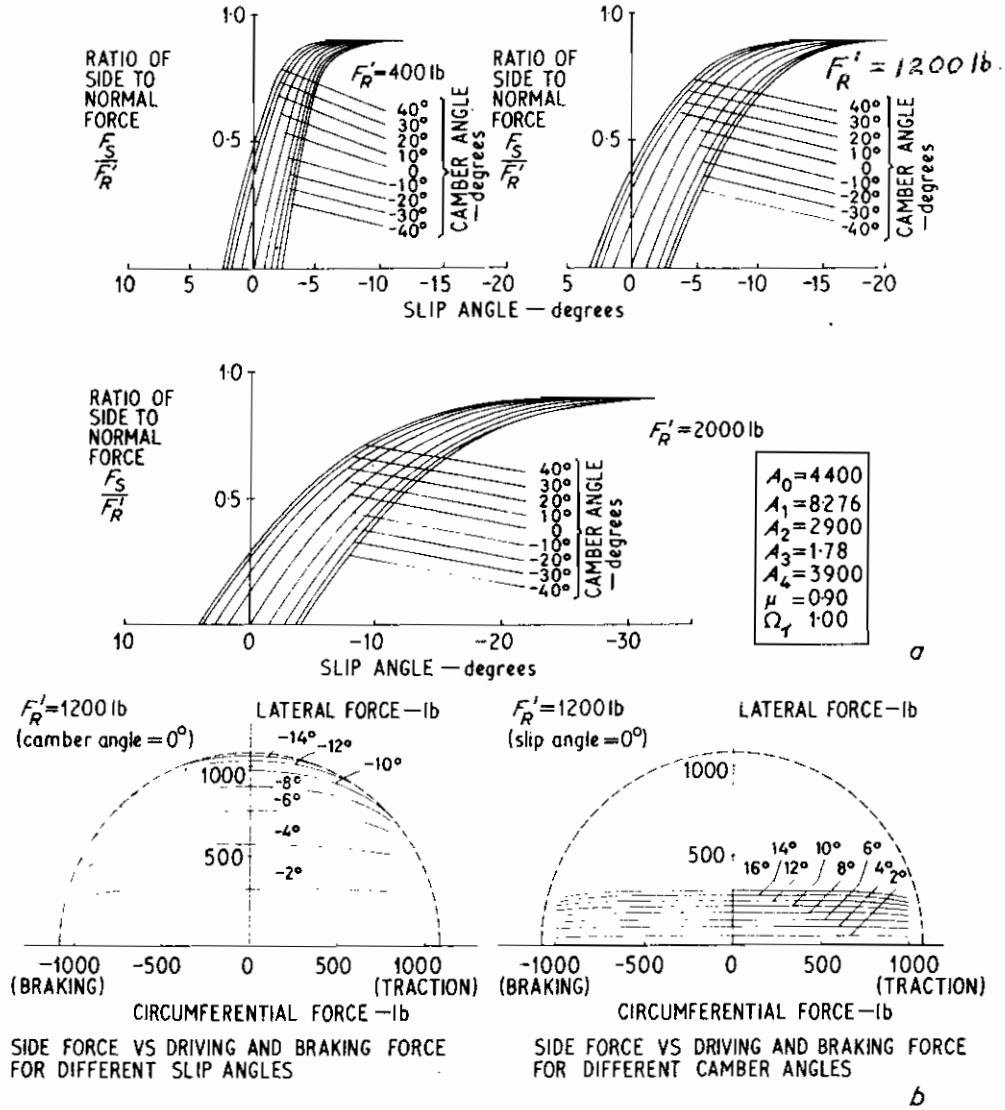

a Ratio of side to normal force versus slip angle for various camber angles.
b Effects of traction and braking on side forces.

Fig. 3.11. Simulated tyre properties

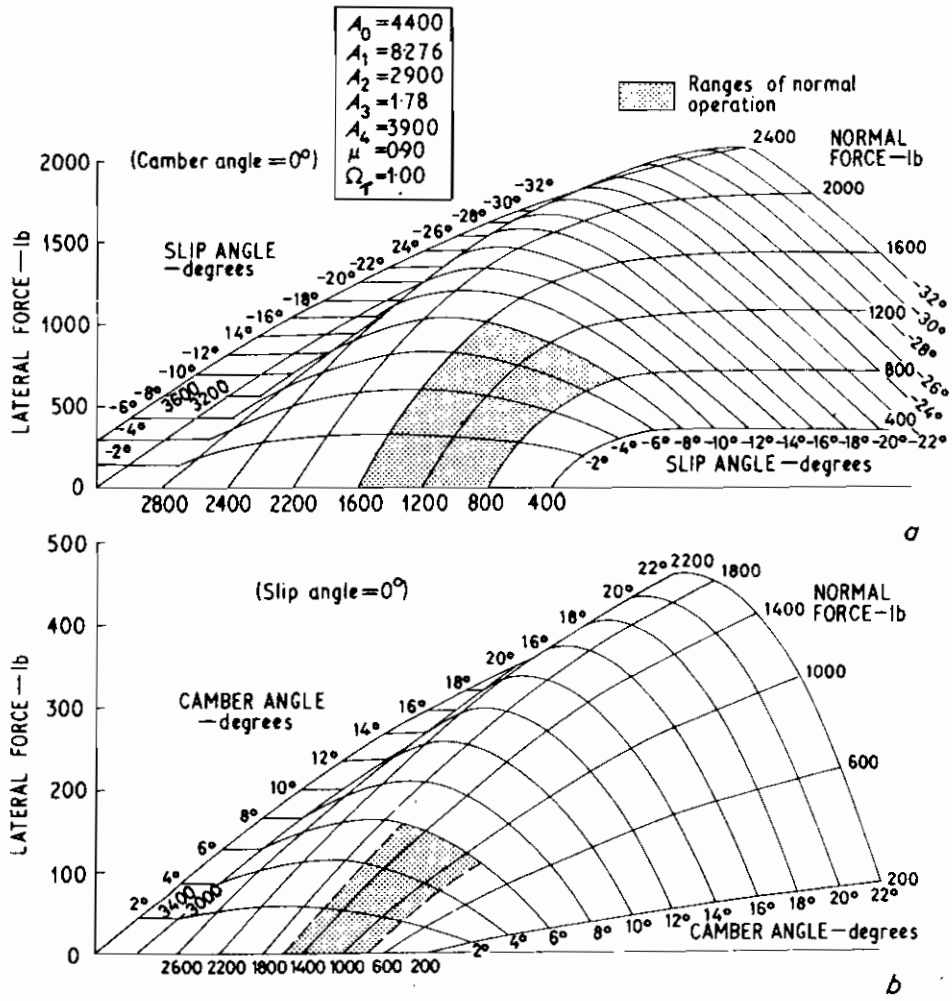

a Lateral force versus slip angle and normal force.
b Lateral force versus camber angle and normal force.

Fig. 3.12

provision made, as yet, for the effects of unequal tyre pressures in the front and rear wheels. Therefore, in each of the reported CAL validation tests, the tyre pressures have been adjusted to be equal. This limitation of the simulation programme can easily be removed when a need arises, since it involves only the addition of appropriate input data.

TERRAIN PROFILE

In the related subroutines that have been developed to date, the terrain is treated as a rigid surface with a uniform friction coefficient. The terrain profile is entered in tabular form in the manner depicted in Fig. 3.13. Note that the tabular input format is used for the case of point-contact representation of the tyres (see under 'Tyre properties', above). The tabular data are interpolated to obtain the elevation and two slopes (Z'_{G_i}, θ_{G_i}, ϕ_{G_i}) at the point directly under each wheel centre. With closely spaced input points, it would be possible to approximate the terrain slopes θ_{G_i} and ϕ_{G_i} from the input values of elevation Z'_{G_i}. However, it was decided to enter the slopes directly in order to achieve accurate control of the interpolated

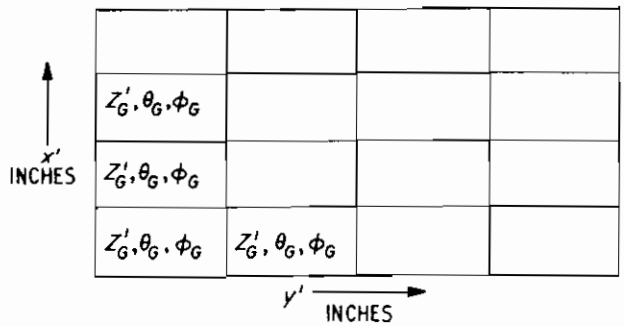

Table of terrain input data.

Euler's angles (θ_G, ϕ_G) define co-ordinate axes that are normal and tangential to the ground surface with $\psi_G = 0$.

Fig. 3.13. Analytical representation of terrain

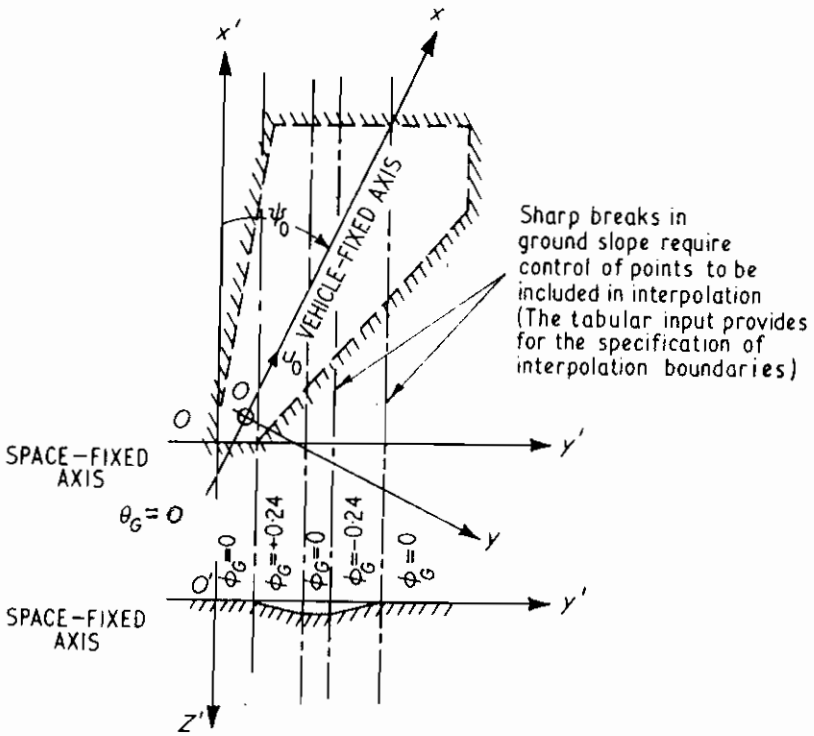

Fig. 3.14. Tabular inputs for embankments and ditches

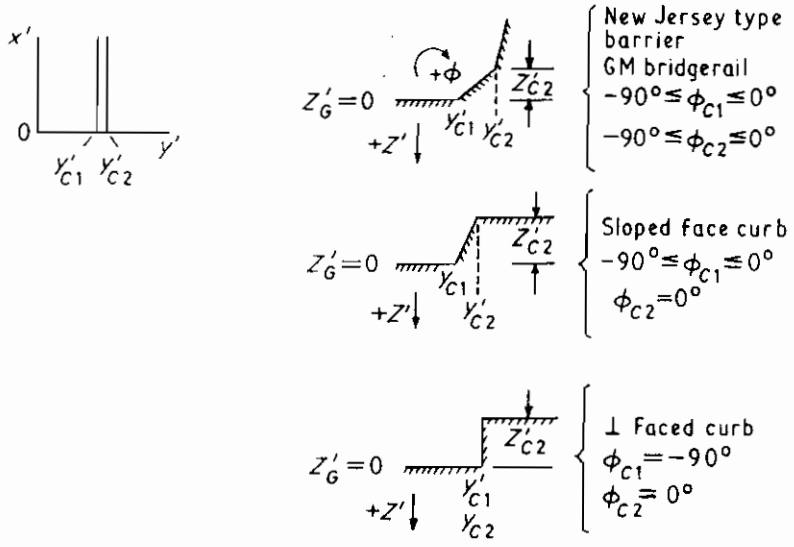

$$\begin{cases} Z'_G = 0, \text{ for } y' < y'_{C1} \\ Z'_G = (y' - y'_{C1}) \tan \phi_{C1}, \text{ for } y'_{C1} \le y' < y'_{C2} \\ Z'_G = Z'_{C2} + (y' - y'_{C2}) \tan \phi_{C2}, y'_{C2} \le y' \end{cases}$$

Fig. 3.15. Analytical representation of kerb profiles

slopes in the case of widely spaced input points. An example of an application of the tabular format to a roadside ditch is depicted in Fig. 3.14.

The present treatment of terrain profile is arbitrarily limited to a 21×21 matrix consisting of 1323 items of data (i.e. three items per terrain point) to define a rectangular segment of terrain. Outside the range of the tabular inputs, the terrain is treated as a flat, horizontal plane. Adjustable boundaries are included within the terrain input tables to provide control of the ranges of interpolation and, thereby, to preclude the inadvertent 'rounding' of abrupt slope changes.

The analytical representation of kerb profiles is depicted in Fig. 3.15. Three planes are defined with lines of intersection parallel to the space-fixed X'-axis. A separate friction coefficient, μ_C, is defined for the kerb facing. The wheels that are not in contact with the kerb are treated as being on a flat, horizontal plane with the specified ground friction coefficient, μ.

CONTROL INPUTS

Open-loop control inputs in the form of steer angle and braking or tractive wheel torques are entered as arbitrary tabular functions of time, which are interpolated in the calculation procedure. The braking and tractive torques are entered separately for the front and rear wheels, but they are applied equally to the left and right wheels at each end of the vehicle. The effects of differential drive gears are simulated for the case of traction (i.e. the torque applied to each of the two wheels of a given pair is limited to the value that spins either of the two wheels).

The input table for the steered angle is abandoned when a kerb is encountered by the wheels, at which time the steer-mode degree of freedom is activated (see 'Degrees of freedom', above). A friction torque is applied in the steer-mode degree of freedom to approximate driver (or remote control) restraint of the steering system.

Some preliminary work has been performed on simple closures of the control loop for path following, but the results have not yet been implemented in the simulation programme.

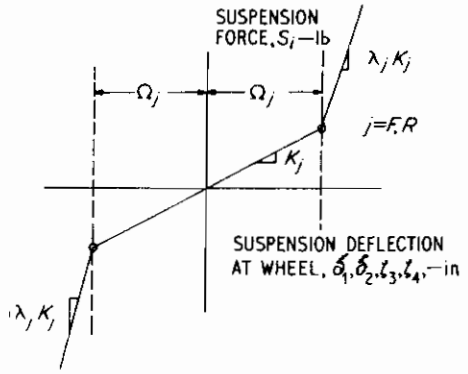

Fig. 3.16. Assumed form of suspension load deflection for zero damping and zero auxiliary roll stiffness

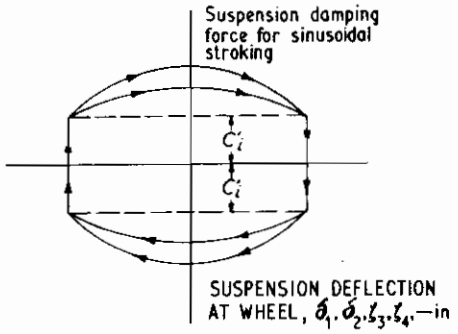

Fig. 3.17. Assumed form of suspension damping

SUSPENSION PROPERTIES

The simulated load-deflection properties of the suspensions, effective at the wheels, include linear elastic rates, elastic deflection-limiting stops, elastic auxiliary roll stiffness, coulomb friction, and viscous damping.

In the interest of simplicity, the deflection-limiting stops are assumed to be symmetrically located with respect to the design position of the suspension and are further assumed to possess constant load-deflection rates (see Fig. 3.16).

The assumed form of damping is depicted in Fig. 3.17. The coulomb friction, C'_i, is used to approximate the combination of 'blow-off' type damping in the shock absorbers and actual friction in the suspension.

COLLISION PROPERTIES OF VEHICLE STRUCTURE

The vehicle sprung mass is treated as a rigid mass surrounded by a layer of isotropic, homogeneous material which exhibits plastic behaviour. The dynamic pressure of the plastic flow process in the peripheral layer of material is assumed to increase linearly with the depth of penetration (see Fig. 3.18).

With these first-approximation assumptions, the force (lb) normal to the contact interface with an obstacle is

$$F_N = K_V \int A \, d\delta$$

where δ is the depth of penetration, in; A the area of contact, in^2; and K_V the property of vehicle structure, lb/in^3.

Inertial effects are neglected in the assumed peripheral layer of material.

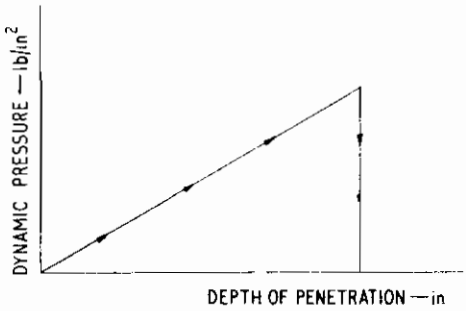

Fig. 3.18. First approximation treatment of collision properties of vehicle periphery

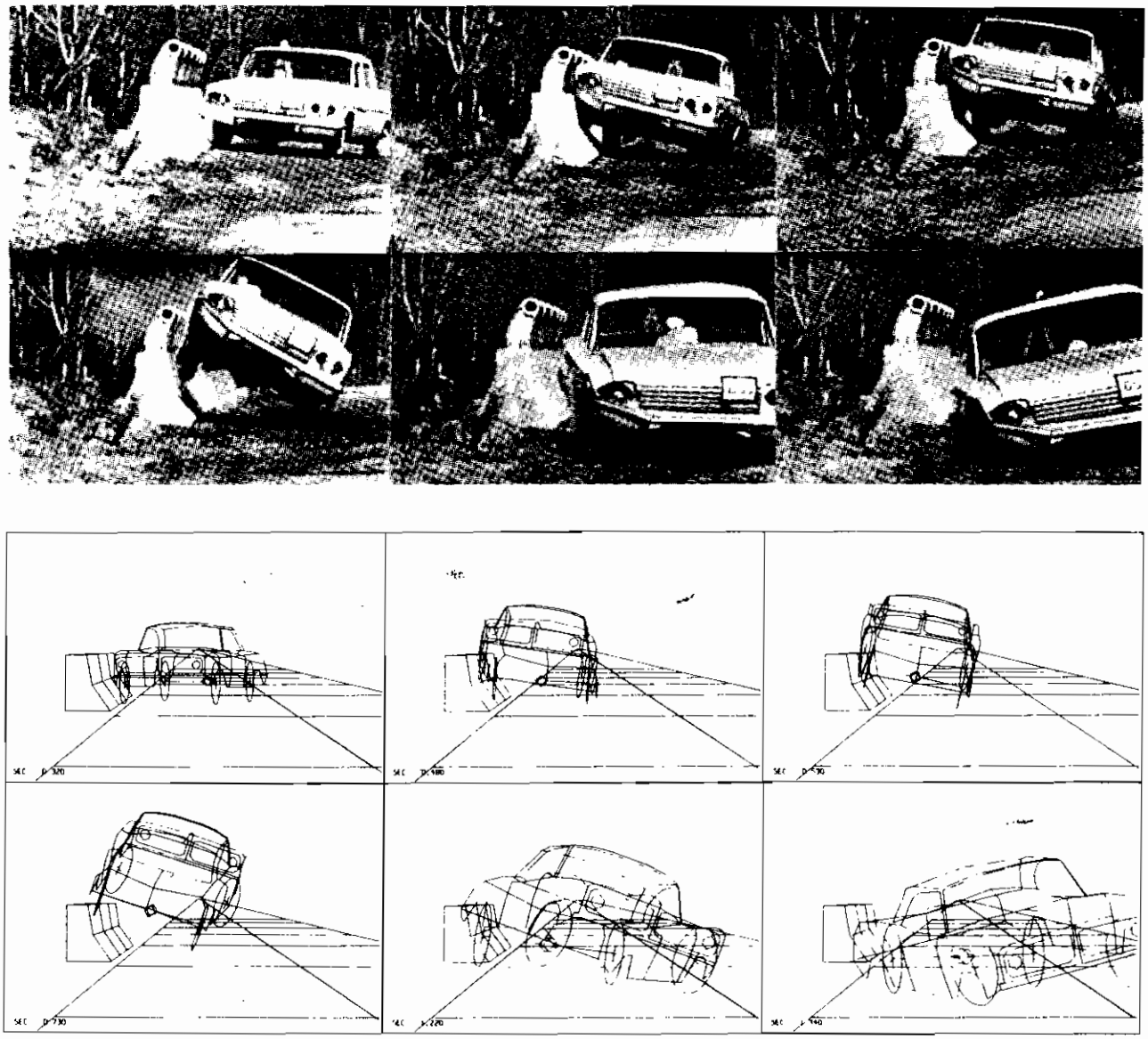

Fig. 3.19. Photographic and computer-graphic displays of GM parapet impact

This seemingly crude representation of the vehicle structural properties appears to be consistent both with the measurements made within the present programme and with the fragmentary data that are available in the literature for moderate depths of penetration (i.e. 12–18 in). If it proves to be successful in achieving an acceptable level of correlation with experiments, its simplicity would appear to be highly desirable in a research programme that is oriented towards the design of roadside devices rather than towards details of vehicle design. The occurrence of larger depths of penetration of vehicle structure, for which the present analytical treatment would not be adequate, might well be interpreted as a failure of the roadside device, since an 18-in penetration corresponds to relatively large applied forces.

COMPUTER-GRAPHICS DISPLAY

An auxiliary computer-graphics display programme has been developed by C. M. Theiss, of CAL; this produces perspective drawings of the simulated vehicle and terrain as seen from selected viewing positions and at selected points in time (**9**). A sample display of violent responses, for one of the gross comparisons of reference (**10**), is presented in Fig. 3.19.

Note that the discrepancies between the predicted and experimental responses displayed in Fig. 3.19 can be attributed, at least in part, to the necessary use in that case of estimated values for vehicle parameters and test conditions (e.g. appreciable resistance to steer changes may have been produced by the remote steering control, whereas a 'hands off' condition was simulated; the extent of tractive

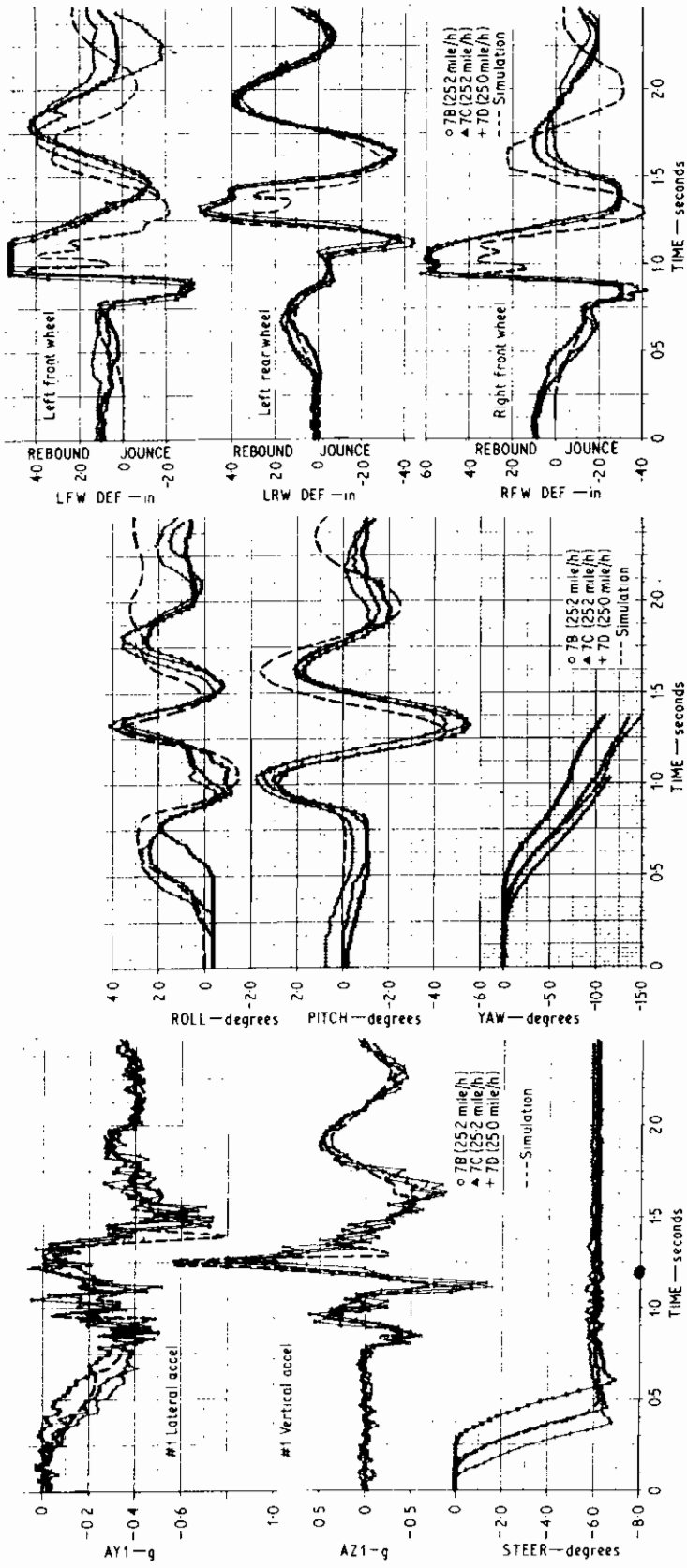

Fig. 3.20. Measured and simulated responses of vehicle traversing 7·1°, 6·75 in high ramp while cornering at 0·4g

effort on the rear wheels was undefined, etc.). It is believed that closer agreement could have been produced by a series of exploratory changes in the estimated inputs. However, an improved correlation achieved by this means could tend to be misleading through the possible mechanism of compensating errors.

The display is produced either on an XY plotter or on a cathode-ray tube. It has been found to be remarkably economical, with a cost of only approximately $0.50 per frame. In the case of the present three-dimensional simulation, that has 11 degrees of freedom, the capability of automatically producing detailed perspective drawings from any viewing position is an extremely valuable aid to understanding the complex motions and to further analytical developments.

DISCUSSION OF RESULTS

A series of preliminary comparisons of predictions of the described vehicle simulation with test results available in the literature is presented in reference (10). The comparisons include cornering, ride, kerb and bridge parapet impact, guardrail impact, ditch traversal, and skidding responses. The generally fragmentary nature of the available response and parameter data limits both the extent and the detail of those comparisons. However, they do provide evidence of generally accurate predictions of vehicle behaviour under a variety of conditions.

During the past year, a special series of tests has been performed by CAL aimed at a rigorous validation of the simulation, with further development being incorporated as required. A description of the test series, which is still

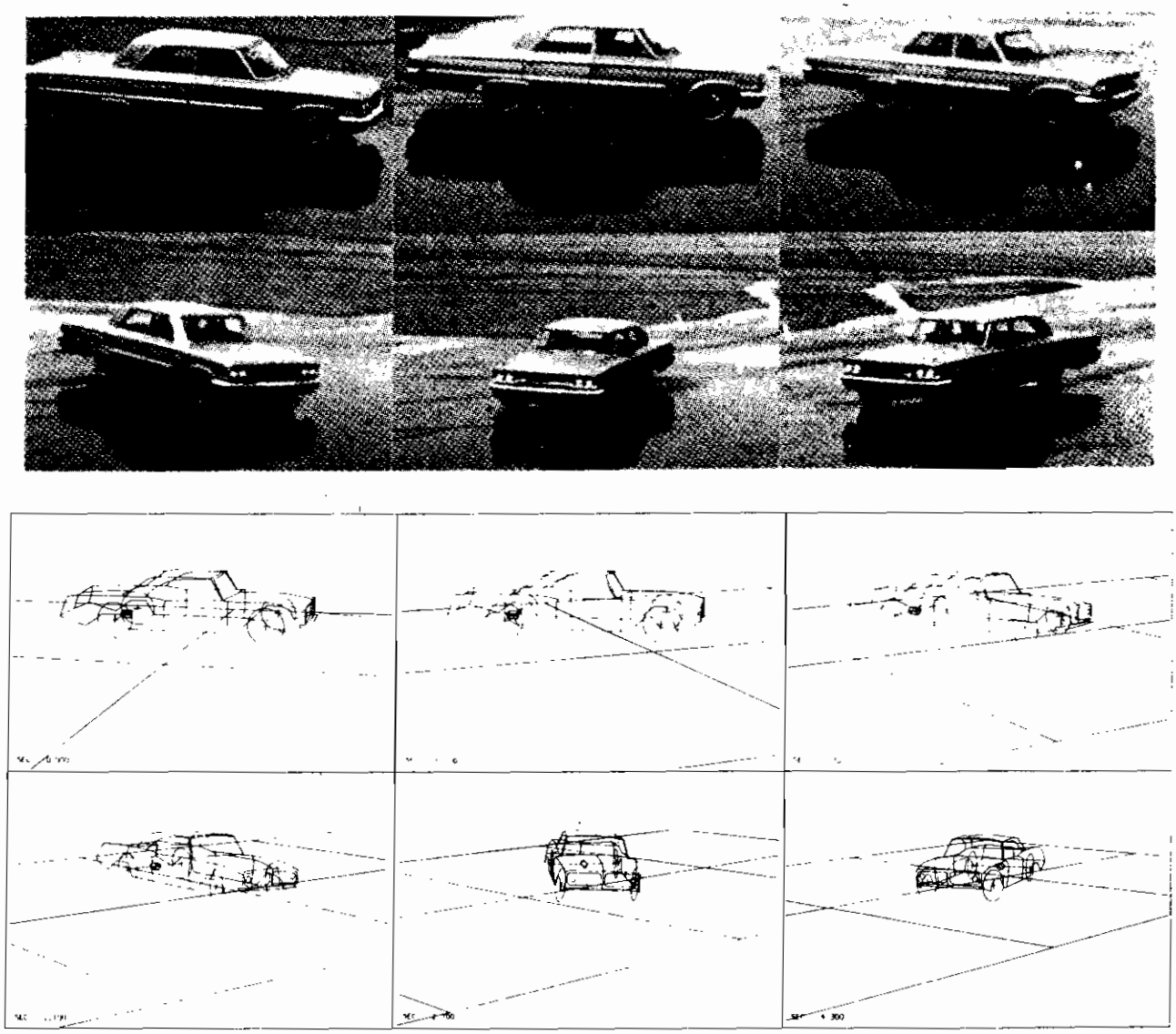

Fig. 3.21. Photographic and computer-graphic displays of a skidding vehicle

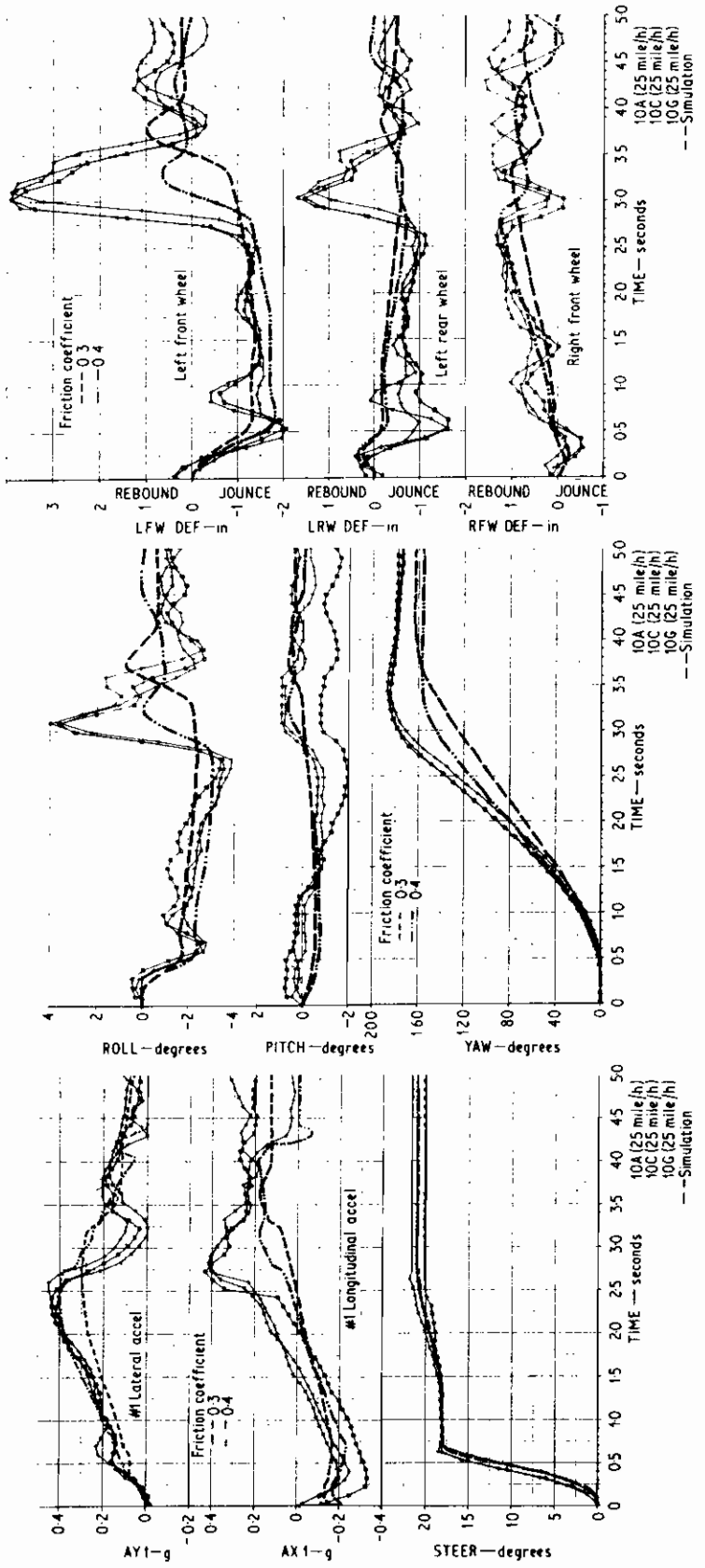

Fig. 3.22. Measured and simulated responses of a skidding vehicle

in progress, and corresponding initial comparisons of predicted and measured responses (some parameter measurements that are being performed by the Ford Motor Company are not yet available) are presented in reference (11). Two of the total of six comparisons of reference (11) are briefly presented here to indicate the level of agreement that has been achieved.

A test condition that is particularly appropriate to the topic of this paper is presented in Fig. 3.20, wherein the test vehicle traversed a 7·1°, 6·75 in high ramp while cornering at 0·4g of lateral acceleration. The test was run with an instrumented 1963 Ford Galaxie four-door sedan at a nominal speed of 25 mile/h. The test was performed three times to establish the repeatability of the measured responses, and the results of all three runs are displayed in Fig. 3.20. The major source of differences among the three experimental responses is believed to have been the slight variation in the timing of the steer control input. The yaw angle oscillograph trace was unfortunately lost approximately 1 s after the initiation of steering. It may be seen in Fig. 3.20 that extremely close agreement has been achieved between predicted and measured vehicle responses in the simultaneous cornering and ride motions. The discrepancies between predicted and measured rebound deflections of the suspensions appear to have been produced primarily by the assumption of symmetrically located and completely elastic deflection-limiting stops in the suspensions (Fig. 3.16).

A comparison of simulated and experimental responses for a skidding manoeuvre is presented in Figs 3.21 and 3.22. In this test condition, the hand brake was used to lock the rear wheels and a large steer input was simultaneously applied. The surface was wetted asphalt, and the nominal vehicle speed was 25 mile/h. Since the friction coefficient could not be determined accurately, simulation results for coefficients of both 0·3 and 0·4 are displayed in Fig. 3.22. The correlation achieved in this manoeuvre is considered to be quite good. The primary sources of error are believed to have been (1) the neglect, in the simulation, of the effects of velocity on the tyre–ground friction coefficient, and (2) a non-uniform roughness of the asphalt surface.

As previously noted, the presented comparisons include some estimated values for vehicle parameters. However, it is emphasized that no exploratory changes, either in estimated parameters or in the assumptions used in formulating the model, have been made in any attempt to achieve improved correlation with the experiments. Vehicle parameters for which known values were available include: total vehicle weight, weight distribution, wheel rates in ride and roll (at the design positions of the suspensions), vehicle dimensions, and tyre properties. Where other specific data were not yet available from the series of measurements being performed by the Ford Motor Company (e.g. moments of inertia), the estimated values have been based on data from several published and unpublished reference sources, and they are believed to be reasonably accurate.

The plan of the present test series is to run progressively more violent manoeuvres, ending with destructive impact tests. A recent sequence of test conditions, more violent than those reported, was performed using the services of skilled stunt drivers from a travelling show. The sequence included forward and reverse skidding on dry pavement, traversal of large ramps alternately by the right and left wheels (Fig. 3.23), and a 50 ft horizontal jump from one ramp to another. Time has precluded the inclusion of data from the described tests for purposes of comprehensive comparisons with predictions. However, a preliminary pictorial comparison of predicted and actual vehicle motions in the jump test is presented in Fig. 3.24. Note that the driver in the jump test, who was apprehensive about the use of an unfamiliar vehicle, selected an excessive speed of 44 mile/h and overshot the landing ramp.

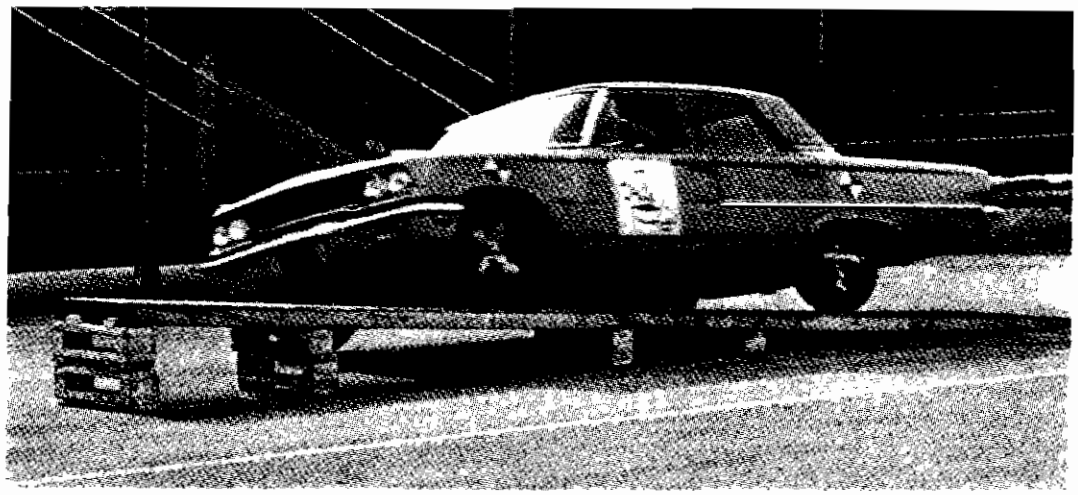

Fig. 3.23. Traversal of large ramps alternately by the left and right wheels

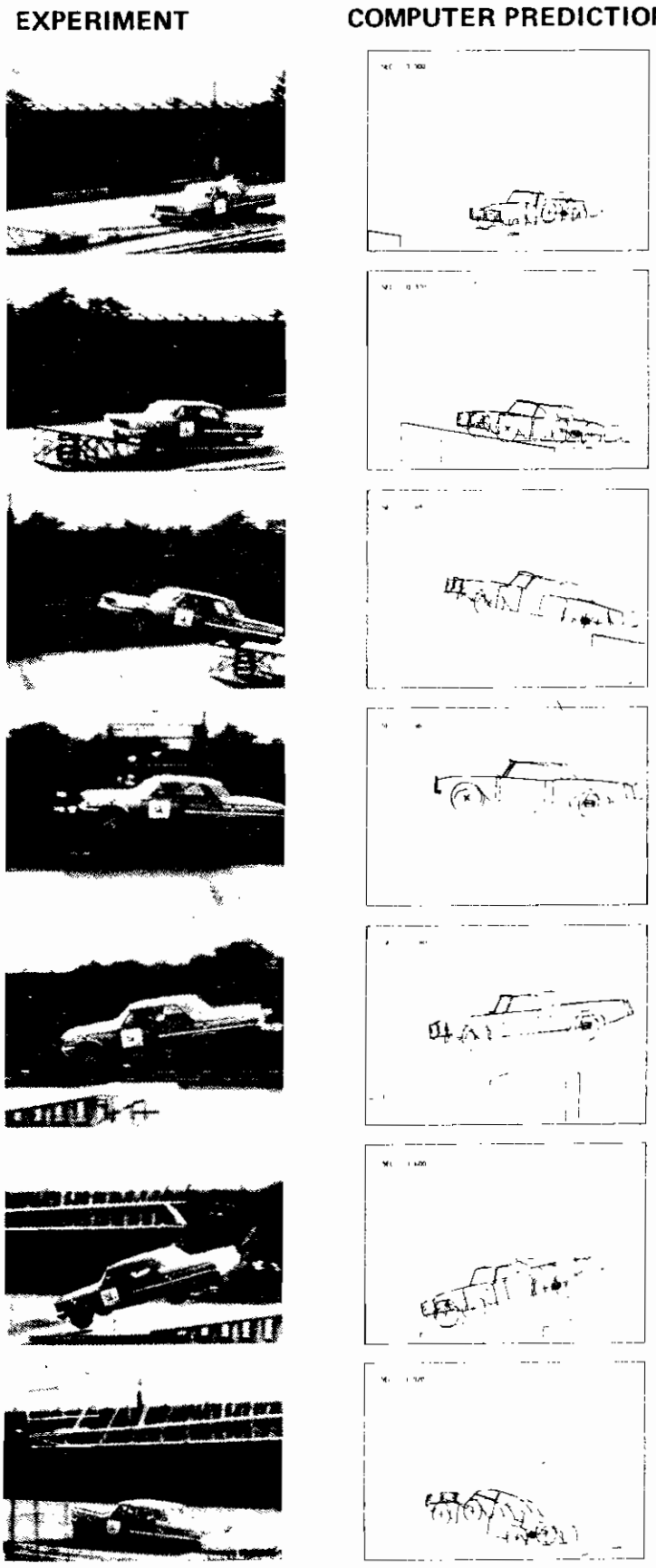

Fig. 3.24. Ramp jump at 44 mile/h

CONCLUSIONS

Excellent correlation of predicted and experimental responses has been achieved in a variety of cornering and ride manoeuvres, both separate and combined, in spite of deliberate related analytical simplifications in the described vehicle model. Also, the operating costs of the computer simulation programme have been found to be surprisingly low for the case of non-impact runs. In view of these facts, a specialized, non-impact version of the computer programme, with improved accuracy in the treatment of tyre and suspension details, is a particularly attractive prospect. Such a modified version of the described programme would appear to be extremely valuable as a vehicle design tool and in studies related to the driving task at the upper limits of vehicle control.

At the present time, emphasis in the CAL research programme is being given to the sprung mass impact aspects of the described simulation. Preliminary gross comparisons of impact predictions with experimental results from the literature have been most encouraging [e.g. see guardrail impact comparison reported in reference (**10**)]. Upon successful completion of the related developments, the computer programme will be ready for the intended applications in the development of physical criteria for roadside energy conversion systems. The large number of variables that influence the consequences of accidentally leaving the roadway (e.g. speed, angle of departure, vehicle size and weight, evasive control inputs, etc.), and the generally poor repeatability and high costs of collision experiments make an analytical supplement a sorely needed aid to roadside design for improved safety.

In addition to the presently intended roadside design application, the fully developed simulation programme may also be suitable to serve as an aid in the reconstruction of actual accidents. By upgrading the accuracy of data obtained from accidents, this proposed application of the computer programme might yield improved information on accident causation and on human tolerances.

ACKNOWLEDGEMENTS

The author wishes to acknowledge the contributions of the following individuals to the research programme described in this paper: *Engineering aspects of the computer simulation*, Messrs N. J. DeLeys and D. J. Segal; *Computer programming*, Mr H. Selib and Mrs Camille F. Fiore; *Computer-graphics displays*, Messrs C. M. Theiss and H. W. Johnson, Jr; *Test performance and data reduction*, Messrs N. J. DeLeys and D. E. Massing; *Vehicle instrumentation*, Messrs D. A. Alianello, D. E. Massing, and W. A. Stahl; *Photography*, Messrs R. L. Jones, R. G. Matthies, and R. J. Kelly.

APPENDIX 3.1

SUMMARY OF EQUATIONS FOR SIDE, BRAKING, AND TRACTION FORCES

The calculation of side, braking, and traction forces is summarized in the following sequence of equations and logic.

1. $T_i = \dfrac{\overline{TQ}_F(12)}{h_i}$, for $i = 1, 2$ (front wheels)

   $T_i = \dfrac{\overline{TQ}_R(12)}{h_i}$, for $i = 3, 4$ (rear wheels)

2. A. If $T_i = 0$, bypass calculation of F_{Ci}, set $F_{C_i} = 0$.

   B. If $0 < T_i$ (traction),

   (1) $F'_{Ci} = \begin{cases} T_i, & \text{for } T_i \leqslant |\mu F'_{Ri}| \\ \mu F'_{Ri}, & \text{for } |\mu F'_{Ri}| < T_i \end{cases}$

   (2) Is any $|\mu F'_{Ri}| < T_i$?

   (*a*) If NO, set $F_{Ci} = F'_{Ci}$.

   (*b*) If YES, compare the corresponding product $(F'_{Ci}h_i)$ for the other wheel of the pair [i.e. the pairs (1, 2) and (3, 4)]. Set the values of the products $(F'_{Ci}h_i)$ in the given pair to the smaller of the individual products. For example, say $F'_{C2}h_2 < F'_{C1}h_1$, then $F_{C2} = F'_{C2}$, and $F_{C1} = F'_{C2}(h_2/h_1)$. (Effects of differential drive gears.)

   C. If $T_i < 0$ (braking),

$$F_{Ci} = \begin{cases} T_i(1 \text{ sgn } u_{Gi}), \\ \quad \text{for } |T_i| \leqslant |\mu F'_{Ri} \cos [\arctan (v_{Gi}/|u_G|) - \psi'_i(1 \text{ sgn } u_{Gi})]| \\ -\mu F'_{Ri}(1 \text{ sgn } u_{Gi}) \cos [\arctan (v_{Gi}/|u_{Gi}|) - \psi'_i(1 \text{ sgn } u_{Gi})], \\ \quad \text{for } |\mu F'_{Ri} \cos [\arctan (v_{Gi}/|u_{Gi}|) - \psi'_i(1 \text{ sgn } u_{Gi})]| < |T_i| \end{cases}$$

(See Fig. 3.10, in which locked-wheel braking is depicted.)

3. A. For $F'_{Ri} \leqslant \Omega_T A_2$,

$$\beta'_i = \frac{A_2A_3(A_4 - F'_{Ri})F'_{Ri}}{A_4[A_1F'_{Ri}(F'_{Ri} - A_2) - A_0A_2]} \times \left[\phi_{CGi} - \frac{2}{\pi}\phi_{CGi}|\phi_{CGi}|\right]$$

$$\bar{\beta}_i = \left[\frac{A_1F'_{Ri}(F'_{Ri} - A_2) - A_0A_2}{A_2\sqrt{[\mu^2(F'_{Ri})^2 - F_{Ci}^2]}}\right] \times \left[\arctan \frac{v_{Gi}}{|u_{Gi}|} + \beta'_i - (1 \text{ sgn } u_{Gi})\psi'_i\right]$$

   B. For $\Omega_T A_2 < F'_{Ri}$,

$$\beta'_i = \left[\frac{A_2A_3\Omega_T(A_4 - \Omega_TA_2)}{A_4[A_1A_2\Omega_T(\Omega_T - 1) - A_0]}\right] \times \left[\phi_{CGi} - \frac{2}{\pi}\phi_{CGi}|\phi_{CGi}|\right]$$

$$\bar{\beta}_i = \left[\frac{A_1A_2\Omega_T(\Omega_T - 1) - A_0}{\sqrt{[\mu^2(F'_{Ri})^2 - F_{Ci}^2]}}\right] \times \left[\arctan \frac{v_{Gi}}{|u_{Gi}|} + \beta'_i - (1 \text{ sgn } u_{Gi})\psi'_i\right]$$

4. A. For $|\bar{\beta}_i| < 3{\cdot}0$,

$$F_{Si} = \sqrt{[\mu^2(F'_{Ri})^2 - F_{Ci}^2]}\,[\bar{\beta}_i - \tfrac{1}{3}\bar{\beta}_i|\bar{\beta}_i| + \tfrac{1}{27}\bar{\beta}_i^3]$$

   B. For $3{\cdot}0 \leqslant |\bar{\beta}_i|$

$$F_{Si} = \sqrt{[\mu^2(F'_{Ri})^2 - F_{Ci}^2]}, \quad \text{where sgn } F_{Si} = \text{sgn } \bar{\beta}_i$$

APPENDIX 3.2

LISTING OF PARAMETER VALUES FOR TEST VEHICLE (1963 FORD GALAXIE FOUR-DOOR SEDAN)

Inertial data

$M_S = 10{\cdot}8180$ lb s^2/in
$M_1 = M_2 = 0{\cdot}3040$ lb s^2/in
$M_3 = 0{\cdot}9450$ lb s^2/in
$I_X = 6000$ lb s^2 in
$I_Y = 30\,000$ lb s^2 in
$I_Z = 36\,000$ lb s^2 in
$I_{XZ} = -192{\cdot}0$ lb s^2 in
$I_R = 600{\cdot}0$ lb s^2 in

Dimensions

a, 54·517 in — b, 64·483 in
Front tread, 61·0 in — Rear tread, 60·0 in

Static distance along the Z-axis between the centre of gravity of the sprung mass and the centre of gravity of the front unsprung masses, 10·138 in.

Static distance along the Z-axis between the centre of gravity of the sprung mass and the roll centre of the rear axle, 12·088 in.

Distance between centre of gravity of rear axle and rear axle roll centre, 2·00 in (roll centre below c.g.).

Distance between spring attachments on rear axle, 46·5 in.

Undeflected wheel radius, R_w, 15·00 in.

Suspension data

Ride rates effective at wheels, for a single wheel, in quasi-linear range:

Front, 131 lb/in — Rear, 192 lb/in

Suspension bumper contact:

Front, ±3·00 in — Rear, ±4·00 in

Coulomb damping:

Front, 55 lb — Rear, 50 lb

Viscous damping coefficient:

Front, 3·5 lb s/in — Rear, 3·9 lb s/in

Auxiliary roll stiffness (i.e. roll stiffness in excess of that corresponding to the front wheel rates in ride and to the rear spring rates and spacing):

Front, 266 000 lb in/rad — Rear, 61 900 lb in/rad
Rear axle roll understeer, 7 per cent

Tyre data

$K_T = 1098$ lb/in
$\sigma_T = 3{\cdot}00$ in
$\lambda_T = 10{\cdot}00$
$A_0 = 4400{\cdot}0$
$A_1 = 8{\cdot}276$
$A_2 = 2900{\cdot}0$
$A_3 = 1{\cdot}780$
$A_4 = 3900{\cdot}0$
} See Fig. 3.25. (Note that the fit to experimental data depicted in Fig. 3.25 could probably be improved by adjustment of the constants. However, the displayed fit is considered to be adequate for the present purposes.)
$\mu = 0{\cdot}30$–$0{\cdot}80$ in the various runs
$\Omega_T = 1{\cdot}00$

APPENDIX 3.3

REFERENCES

(1) MILLIKEN, W. F., WHITCOMB, D. W., SEGEL, L. *et al.* 'Research in automobile stability and control and in tyre performance', *Proc. Auto. Div. Instn mech. Engrs* 1956.
(2) BUNDORF, R. T., POLLOCK, D. E. and HARDIN, M. C. 'Vehicle response to aerodynamic inputs', *Res. Pub. GMR-403* 1963 (June) (General Motors Corporation).

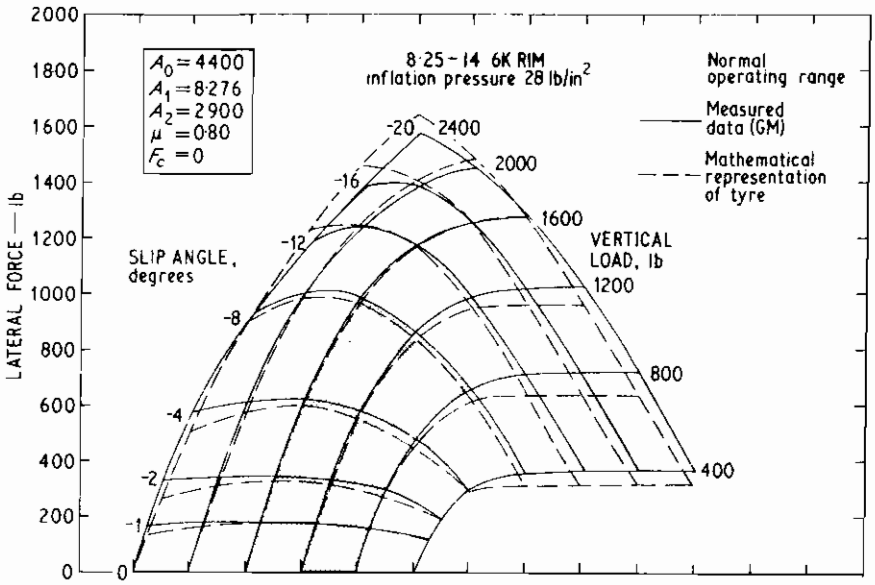

Fig. 3.25. Lateral force versus slip angle and vertical load

(3) WEIR, D. H., SHORTWELL, C. P. and JOHNSON, W. A. 'Dynamics of the automobile related to driver control', *Tech. Rept No. 157-1* 1966 (July) (Systems Technology, Inc.).
(4) ETKIN, B. *Dynamics of flight* 1959, Chap. 4 (Wiley, New York and London).
(5) KNIGHT, K. E. 'Evolving computer performance 1963–1967', *Datamation* 1968 (January), 31.
(6) ALBERT, C. J. 'A method of simulating tyre enveloping power in calculations of vehicle ride performance', *CAL Rept No. YM-1424-V-300* 1961 (November).
(7) RADT, H. S. and MILLIKEN, W. F. 'Motions of skidding automobiles', S.A.E. Paper No. 205A 1960 (June).
(8) KREMPEL, G. 'Preliminary results from tests on automobile tyres', Dissertation, Universitat Karlsruhe 1965 (in German).
(9) THEISS, C. M. 'A computer aided movie-producing program for the simulation program of roadside energy conversion systems', *CAL Rept No. VJ-2251-V-2* 1967 (November).
(10) MCHENRY, R. R., SEGAL, D. J. and DELEYS, N. J. 'Computer simulation of single vehicle accidents', *Stapp Car Crash Conf., Anaheim, California* 1967 (October).
(11) DELEYS, N. J. 'Validation of a computer simulation of single vehicle accidents by full-scale testing', *First Int. Conf. Vehicle Mechanics, Wayne State University* 1968 (July).

HANDLING OF VEHICLES UNDER EMERGENCY CONDITIONS

Mr R. R. McHenry—In reply to Mr Watts, regarding the measurement of suspension characteristics, the wheel rates in ride and roll and the friction values were measured on the assembled vehicle. The shock absorbers were measured as separate components and their measured installation ratios were applied in the development of corresponding parameter values for the computer simulation. We were not able to obtain direct measurements of load deflection properties of the suspension bumpers (i.e. the wheel travel limit stops) within the present research programme, but we have used measured clearances to the stops. The variation of front wheel camber with suspension position was measured on the vehicle.

To further clarify the matter of vehicle parameters, it seems appropriate to elaborate on our general approach. One of our objectives in the present research programme has been to apply each item of the vehicle parameters in a directly measurable form. Since it is a common practice in mathematical modeling to define 'equivalent' parameters and to adjust the values to achieve correlation with experimental data, we have gone to some lengths to distinguish the present approach. We let a subcontract to the Ford Motor Company in Dearborn, Michigan, for measurement of the vehicle parameters, and the results of their measurements (only partially available at the time the paper was written) have been used directly in all of the simulation runs. The tyre properties were measured by the General Motors Engineering Staff and were also applied directly.

By means of the direct use of parameters as measured by disinterested individuals, we have hoped to make it very clear that the correlation with experimental responses is genuine, involving no 'tune-up' of the simulated vehicle properties. The most recent technical report on the research programme (CAL Report No. VJ-2251-V-3, December 1968) summarizes the results of the vehicle parameter measurements and presents comparisons between predicted and experimental responses for a total of ten different vehicle manoeuvres.

In reply to Mr Sharp regarding the lateral kinematic properties of the suspension system, we have not yet included any lateral compliance in the simulated suspensions. As far as inertial interactions between the sprung and unsprung masses are concerned, we have assumed simple constraints that are described under 'degrees of freedom' in the paper. Front wheel camber is treated as a tabular function of suspension position, and rear axle roll steer is treated as a linear function of the angular degree of freedom of the rear axle. Thus, we are treating the suspension geometry in some detail.

I am aware of the current emphasis being given to compliance steer effects. However, on the basis of the correlation achieved with experimental responses within the present research programme (presented in detail in CAL Report No. VJ-2251-V-3, December 1968), I must conclude that compliance steer effects are of secondary importance, at least in the relatively violent manoeuvres that have been investigated.

In reply to Mr French, regarding the force levels with which ordinary drivers can cope, I have seen some recent unpublished experimental results that were obtained with instrumentation installed in automobiles without knowledge of the drivers. Those results indicate that 0·3*g* is the maximum value of cornering acceleration that is used in normal driving on American highways. However, the conditions that we are simulating are not, of course, normal driving. Rather they correspond to violent evasive manoeuvres. While I cannot shed any light on the upper limits of driver capabilities, I would like to point out that the primary interest of our sponsor (the U.S. Bureau of Public Roads), in relation to the described simulation, lies in the design of the roadside. Therefore, while the upper limits of control are of definite interest, the vehicle trajectory after control loss, as influenced by terrain features and obstacles, is of equal interest.

In reply to Professor Macmillan, regarding self-generated rollovers, we have not yet attempted to simulate such occurrences.

Of particular personal interest, in relation to this topic, would be the introduction of an independent rear suspension into the computer simulation and the subsequent performance of runs with combinations of brake-induced pitching and hard cornering on irregular terrain. The required changes in the computer programme would actually constitute simplifications, in view of the relatively complicated equations for the solid rear axle.

HANDLING OF VEHICLES UNDER EMERGENCY CONDITIONS

LOUGHBOROUGH · 8th JANUARY 1969

A SYMPOSIUM

arranged by

The Automobile Division, The Institution of Mechanical Engineers

in association with

The University of Technology, Loughborough

PUBLISHED BY THE INSTITUTION OF MECHANICAL ENGINEERS

1 BIRDCAGE WALK · WESTMINSTER · LONDON SW1